JOURNAL OF SOLID STATE CHEMISTRY 107, 108–116 (1993)

Trirutile Phases of $HTaWO_6 \cdot xH_2O$: Vibrational Properties and Electrical Conductivity

M. CATTI,* E. CAZZANELLI,† C. M. MARI,* AND G. MARIOTTO†‡

*Dipartimento di Chimica Fisica ed Elettrochimica, Università di Milano, Via C. Golgi 19, 20133, Milan, Italy; and †Dipartimento di Fisica, Università di Trento, 38050 Povo, Trento, Italy

Received October 12, 1992; in revised form March 1, 1993; accepted March 3, 1993

The phases of $HTaWO_6 \cdot xH_2O$ ($x = 3/2, 1/2, 0$) system with trirutile structure, including fully anhydrous $TaWO_{5.5}$, were characterized by X-ray and thermoanalytical methods and investigated by Raman scattering and complex impedence spectroscopy. The vibrational study involved the $LiTaWO_6$ precursor as well. Raman spectra show an evolution correlated with progressive water loss after selective heat treatments, up to 900°C. In some conditions, a disordered modification of $TaWO_{5.5}$ appears in the spectra even below 300°C. The ionic conductivity is smaller than in the pyrochlore polymorph and can be ascribed to a lower mobility of H^+ ions in the trirutile structure, with an activation energy of 0.35 eV. © 1993 Academic Press, Inc.

1. Introduction

The hydrogenated oxydes of the class $HM^{V}M^{VI}O_6$ have been synthetized in recent years and studied for their interesting protonic conductivity. They can be obtained via ionic exchange from corresponding alkali compounds. In particular, for $HTaWO_6$ and $HNbWO_6$, three basically different structures are reported, related to the conventional pyrochlore (*1–5*), trirutile (*6*), and ReO_3 (perovskite) (*7*) structure types, respectively. In all of these crystal forms, water molecules are contained in variable amount.

A complex evolution occurs when $HTaWO_6 \cdot xH_2O$ is obtained by replacing Li^+ cations by protons in $LiTaWO_6$, which exhibits a trirutile crystal structure, characterized by corner-sharing and edge-sharing octahedral units packed into a layered configuration (*8*). According to details of the ion-exchange reaction, either an isostructural trirutile-type form (*6*) or a ReO_3-type modification (*7*) of $HTaWO_6 \cdot xH_2O$ is obtained, with a variable amount of structural water. In the former case, the acidic protons and the water molecules are located between the oxide layers (*6*), i.e., in the same regions formerly occupied by Li^+ ions. A preliminary Raman study of the trirutile polymorph (*9*) has revealed the existence of a fully dehydrated, highly disordered form, which is obtained by laser irradiation or by thermal annealing of either the pyrochlore or the trirutile modification itself.

Electrical conductivity measurements are available for the pyrochlore phase of $HTaWO_6 \cdot xH_2O$ (*1*), but not for the other crystal modifications. A peculiar dependence of the conductivity on temperature has been found and related to progressive dehydration of the pyrochlore. However, according to a detailed theoretical analysis of the mechanism of proton motion of thermally activated hopping (*10*), an active role of structural water molecules in the conduction

‡ Email: MARIOTTO@ITNCISCA (Bitnet); MARIOTTO@ITNVAX.SCIENCE.UNITN.IT (Internet).

0022-4596/93 $5.00

process has been ruled out, in agreement with previous Raman findings (*5*).

A new study of the trirutile modification of $HTaWO_6 \cdot xH_2O$ is presented here, with the aim of clarifying some of the open points concerning its electrical and vibrational behavior.

2. Experimental and Results

2.1. Preparation and Phase Relations

The lithium precursor $LiTaWO_6$ was synthetized by solid-state reaction of a mixture of Li_2CO_3, Ta_2O_5, and WO_3 in stoichiometric ratio (*11*). The reagents were calcined in air at 800°C for 12 hr twice, with an intermediate grinding step. X-ray powder diffraction proved the product to be single-phase $LiTaWO_6$ with a trirutile-type pattern. This compound was proton exchanged in a 4 *M* HNO_3 solution for 48 hr at 80°C, with an intermediate substitution of the acid (*6, 12*). Care has to be taken in this preparation step, because using more severe conditions (typically, 13 *M* H_2SO_4 at 200°C) can lead to formation of $HTaWO_6 \cdot H_2O$ with perovskite-type structure (*7*). Complete Li^+/H^+ exchange was checked by lithium analysis in solution by atomic absorption spectrophotometry.

The crystallographic and thermal characterizations of all samples were performed by a Siemens D-500 X-ray powder diffractometer (Cu$K\alpha$ radiation, scan speed of 1°(2θ)/min), and by a Netzsch thermoanalyzer (TGA + DTA, heating rate 5°C/min). The diffraction pattern of the fresh polycrystalline powders obtained after ion exchange corresponded to pure $HTaWO_6 \cdot 3/2H_2O$ with trirutile-type structure [a = 4.710(9) Å, c = 25.80(5) Å]. A thermal study by thermogravimetric and differential thermal analysis, coupled with isothermal treatments at different temperatures in a furnace and subsequent X-ray diffraction on the samples confirmed substantially the phase relations obtained by the previous investigation (*6*). The dehydration reactions occurring can be summarized as follows:

$$HTaWO_6 \cdot 3/2H_2O \rightleftarrows HTaWO_6 \cdot 1/2H_2O + H_2O \quad (30\text{–}80°C),$$

$$HTaWO_6 \cdot 1/2H_2O \rightleftarrows HTaWO_6 + 1/2H_2O \quad (120\text{–}220°C),$$

$$HTaWO_6 \rightarrow TaWO_{5.5} + 1/2H_2O \quad (220\text{–}400°C).$$

The hemihydrated phase has a small but well defined range of thermal stability. Its diffraction pattern, though similar to that of $HTaWO_6 \cdot 3/2H_2O$, shows a number of peculiar peak shifts which are diagnostic, consistently with the significant shortening of the c cell edge. On the other hand, the stability range of the pure dehydrated phase in air appears to be vanishing, with an X-ray powder pattern which resembles very closely that of the hemihydrated phase.

2.2. Electrical conductivity

The measurements were performed on pellets covered by thin Pt films sputtered on both sides. A Solartron complex admittance apparatus was employed, using frequencies in the range 1–3 × 10^5Hz. Circles on the complex impedence plane appeared clearly, and the conductivities σ were obtained from a high-frequency intercept with the real axis. The measuring procedure was repeated at several temperature values in the range 25–200°C in air, obtaining the Arrhenius-type plot of log (σT) versus $1/T$ shown in Fig. 1. A complex multiphase shape appears, similar to that obtained for the pyrochlore polymorph of $HTaWO_6 \cdot xH_2O$ (*1*); however, here the correspondence between regions of the curve and hydration of the compound is different. In fact, by taking into account the results of the thermal study, the bottom of the curve can be ascribed to the pure hemihydrate phase, while the low- and high-T branches should correspond to $HTaWO_6 \cdot 3/2H_2O$–$HTaWO_6 1/2H_2O$ and $HTaWO_6 \cdot 1/2H_2O$–$HTaWO_6$ two-phase systems, respectively. On the other hand, in the pyrochlore case we had a continuous dehydration of $HTaWO_6 \cdot H_2O$ in the low-T

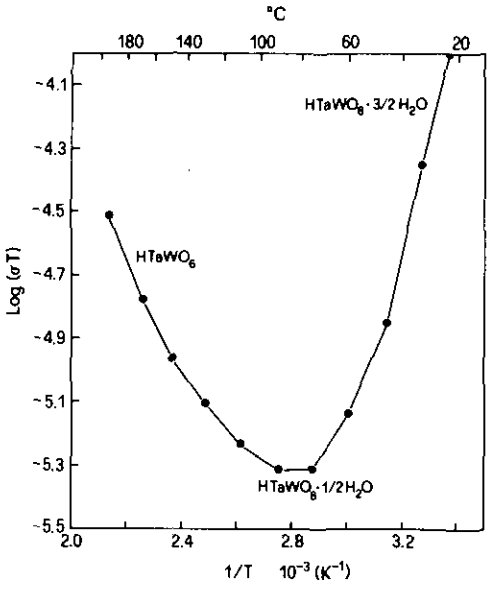

FIG. 1. Arrhenius plot of the conductivity values for $HTaWO_6 \cdot xH_2O$ pellets, measured in air, between 25 and 200°C.

region, and a stability range of single phase $HTaWO_6$ in the high-T branch of the curve (*1*).

According to the interpretation of pyrochlore results (*1*), in the low-T region the electrical conductivity should be mainly ascribed to H^+ transport via H_2O molecules, probably related to grain-boundary humidity (*12*). This explains the decreasing trend of $\sigma(T)$, due to dehydration. In the high-T region, on the other hand, the dehydration effect is overcompensated by the Arrhenius-like enhancement of conductivity on temperature. An increase of $\log(\sigma T)$ versus $1/T$ is produced, which becomes linear only after complete loss of water, when charge transport occurs by thermally activated hopping of acidic H^+ ions. The activation energy for the latter process ($T > 150$°C) is computed to be 0.39 eV. In order to better characterize the electrical behavior of the anhydrous phase $HTaWO_6$, conductivity measurements were repeated in dry argon atmosphere within the T range 80–190°C. Unlike the air results, now the Arrhenius plot shows a neat linear behaviour (Fig. 2); this is ascribed to conduction of the acidic H^+ proton with activation energy of 0.35 eV, in reasonable agreement with the previous result obtained in a narrower temperature range.

By extending the measurements in air up to 300°C, the data obtained show the left-hand part of the parabola-like curve of Fig. 1 to go on raising with positive deviation from linearity. Thus the third dehydration step ($HTaWO_6 \rightarrow TaWO_{5.5} + 1/2H_2O$) appears to occur continuously over a temperature range, with no clear-cut slope change in the Arrhenius plot (two-phase behavior). From the study of the corresponding pyrochlore system (*1, 13*), it can be inferred that a more thorough understanding of the conductivity of these hydrated compounds can be obtained only by carefully controlling the water vapor pressure in the atmosphere.

2.3. Raman Scattering: Measuring Procedures

For the annealings of $LiTaWO_6$, a piece of pellet in a quartz container inside a furnace was used. The time elapsed to cool down to room temperature was at least 1

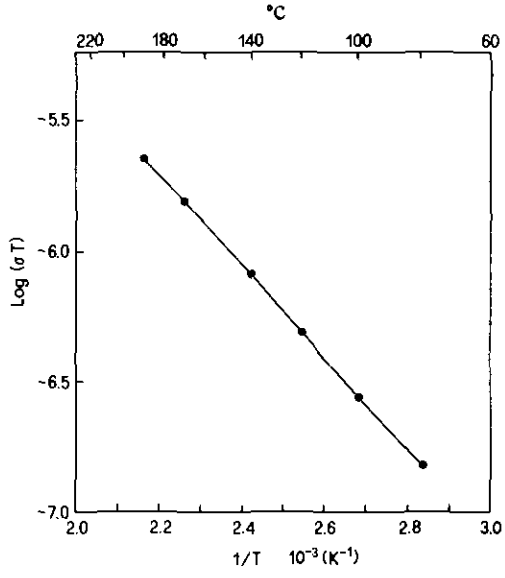

FIG. 2. Arrhenius plot as in Fig. 1, but performed in a dry argon atmosphere, between 80 and 190°C.

hr. For the powders of hydrogenated compounds the annealings were performed either in open quartz containers or in glass capillaries. To reintroduce water in samples dehydrated previously, the powders were suspended in water, stirred and then maintained at 60–80°C until complete evaporation of the liquid. The same method was applied to deuterate some samples, using D_2O instead of normal water. Samples were always kept in air both during and after thermal treatments.

Raman spectra were excited by either 514.5- or 488.0-nm lines of an Ar^+ ion laser. To avoid possible decomposition of the samples the laser powers were typically maintained at about 100 mW or less; the time required to collect a Raman spectrum in the region between 0 and 1200 cm^{-1} was about 15 min. The scattered light was dispersed by a Jobin–Yvon double monochromator HG-2S with holographic gratings (2000 grooves per mm) and detected by a standard photon counting system. The experimental resolution was about 3 cm^{-1} for most of spectra.

The real temperature of samples under irradiation in thermal equilibrium conditions was estimated (with an error of 10–20°C) through the anti-Stokes-to-Stokes intensity ratio of the Raman modes between +200 and −200 cm^{-1}, taking in account also the intensity dependence on the frequency of the scattered light (*14*).

2.4. *Raman Spectra of Trirutile $LiTaWO_6$*

The Raman spectrum of the salt $LiTaWO_6$ with a trirutile structure, parent of the protonated compound, is reported in Fig. 3. The large number of the peaks and their sharpness are consistent with a quite ordered crystal structure where atoms occupy low symmetry sites. However, a normal modes assignment is not allowed by lack of well oriented monocrystalline samples.

The very strong peak at 960 cm^{-1}, with the associated feature in the range 900–930 cm^{-1}, is not observed in the spectra of isomorphous trirutile-like MTa_2O_6 compounds

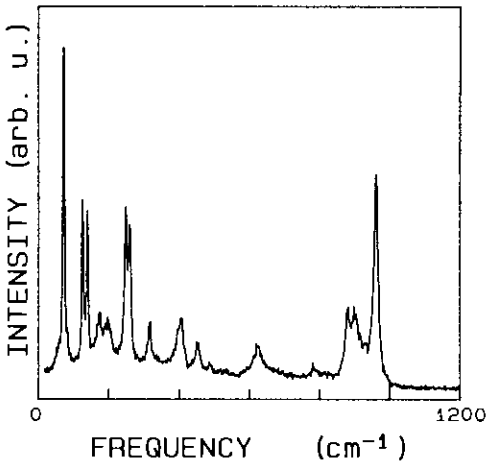

FIG. 3. Room-temperature Raman spectrum of $LiTaWO_6$ untreated polycrystalline sample.

(*15, 16*), where stretching modes of TaO_6 octahedra are reported to lie in the 700 cm^{-1} region. On the other hand, comparable high frequency peaks are shown by $TiTa_2O_7$ (*17*), with different space group, and are assigned to the stretching mode of edge-sharing TaO_6 octahedra.

In agreement with thermogravimetric and DSC measurements, which do not reveal any phase transition at higher temperature, the vibrational spectrum of $LiTaWO_6$ remains remarkably constant after thermal treatments up to 800°C, as well as after strong laser irradiations performed in air.

2.5. *Raman Spectra of Trirutile $HTaWO_6 \cdot xH_2O$*

2.5.1. Hydrated phases. The transformations of the hydrogenated trirutile depend mainly on the water content; in order to explore by Raman spectroscopy all phase changes, powder samples were synthetized at different times and repeatedly measured after each heat treatment. A typical, well reproducible spectrum obtained at "room temperature" in air, on freshly exchanged, untreated powders is shown in Fig. 4a. A general broadening for all the spectral features can be observed, with respect to the parent $LiTaWO_6$; in addition, the sequence

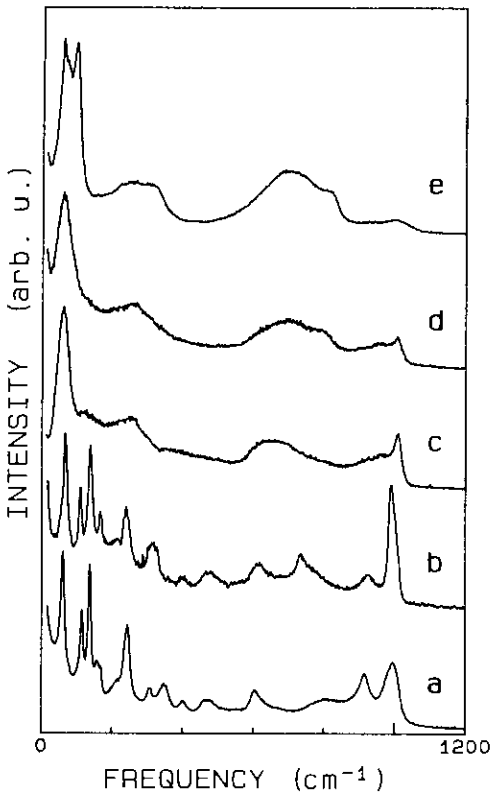

FIG. 4. Room-temperature Raman spectra of the different phases derived from $HTaWO_6 \cdot xH_2O$: (a) untreated powders, hydration state between $HTaWO_6 \cdot 3/2H_2O$ and $HTaWO_6 \cdot 1/2H_2O$; (b)powders heated for 65 hr at 150°C, sample composition $HTaWO_6$; (c) powders after 17 hr at 440°C, fully dehydrated phase $TaWO_{5.5}$; (d) powders after heating for 22 hr at 700°C; and (e) powders after heating for 20 hr at 900°C.

of Raman peaks of Fig. 3 is conserved in the exchanged compound, showing only a systematic downshift of about 10 cm^{-1} and an upshift of 35 cm^{-1} for most of the low-frequency and high-frequency modes, respectively.

An unexpected, new spectral feature appears in the region 300–370 cm^{-1} for the $HTaWO_6 \cdot xH_2O$ samples; it shows an evolution strongly correlated to the thermal history of the samples, henceforth to the water content, which is discussed in detail in the next section.

The internal modes of the intercalated water give very weak and not always reproducible Raman spectra: the bending mode can be identified with the band barely observable at about 1600 cm^{-1} in some samples. The region of the O–H stretching modes presents broad and weak features, whose intensity is significantly sample dependent. However, all untreated powders, exhibiting the spectral shape of Fig. 4a for the host matrix modes, show in the O–H stretching region two very broad features, with maxima at about 2800 and 3400 cm^{-1} (see Fig. 5a). The same two modes are also observed in IR spectra, once again showing weak intensity and broad shape.

No isotopic-shift effects were observed in deuterated samples directly related to librational modes of the water molecule. Thus water would only be involved in vibrational modes relating large structural units.

All samples of freshly exchanged powders, measured in air, had an estimated temperature (see Section 2.3) between 85 and 125°C, due to the heating effect of the laser. Thus, according to the phase relations of

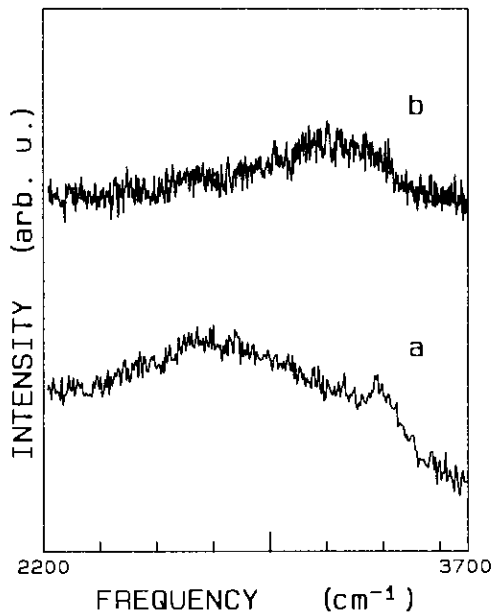

FIG. 5. Raman spectrum in the region of O–H stretching: (a) freshly exchanged powders and (b) sample heated 20 hr at 300°C, corresponding to $HTaWO_6$ phase.

Section 2.1, the Raman spectra of Fig. 4a are likely to probe an intermediate state between $HTaWO_6 \cdot 3/2H_2O$ and $HTaWO_6 \cdot 1/2H_2O$.

2.5.2. Spectral evolution under moderate heating. Heatings below 100–120°C are comparable for their effects to low-power laser irradiation (about 100 mW); they produce only small variations in the bandwidths and relative intensities, in comparison to spectrum of Fig. 4a.

For thermal treatments of the initial hydrated phase between 120 and 300°C, the changes of Raman spectrum appear erratic and scarcely reproducible. However, many experiments on different samples indicate two main routes of structural evolution. In the first case, spectra of a strongly disordered phase are observed; this phase, labeled β, is discussed below. The other transformation (Fig. 4b) implies much less relevant changes of the Raman spectrum, i.e.:

(i) The lowest frequency mode shifts from 61 to 67 cm^{-1}.

(ii) The splitting of the doublet 115–137 cm^{-1} of the hydrated samples increases slightly, giving typical values of 110–140 cm^{-1}. This effect seems to be partially reversible after some months exposition to air.

(iii) The relative intensity of the 240-cm^{-1} peak decreases after dehydration.

(iv) The band at about 350 cm^{-1} changes its intensity and its energy under desiccation processes (Fig. 6). For strongly hydrated samples it lies at about 365 cm^{-1}, with a remarkable intensity (Fig. 6a). For moderate heating both frequency and intensity decrease progressively; indeed, for dehydrated $HTaWO_6$ samples the band appears more or less overlapped with that at 310 cm^{-1} (Fig. 6c). A significant direct involvement of the water molecule in the eigenvector of this mode can be ruled out by measurements on deuterated samples, where a peak frequency of 363 cm^{-1} is observed, as in strongly hydrated materials.

(v) The broad shoulder centered at about 800 cm^{-1} in the fully hydrated phase shifts to lower frequency and increases its intensity as a consequence of the heating. For the samples treated at 300°C, which can be considered totally transformed, the band maximum lies at about 740 cm^{-1}.

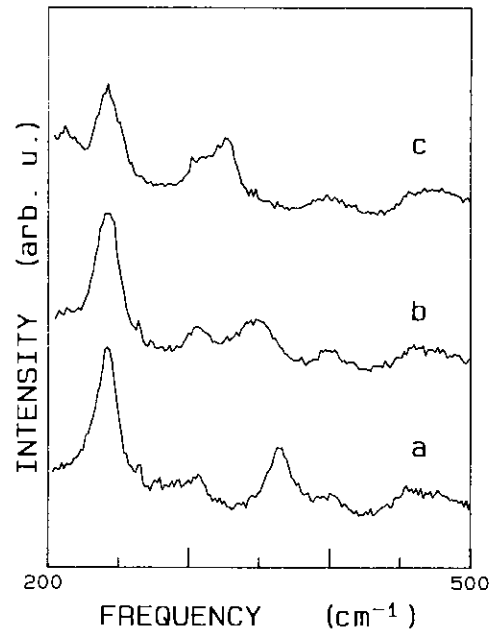

FIG. 6. Dependence on water content of the host matrix Raman spectrum in the range 200–500 cm^{-1}: (a) powders in equilibrium with liquid water, hydration state close to $HTaWO_6 \cdot 3/2H_2O$; (b) untreated powders, hydration state between $HTaWO_6 \cdot 3/2H_2O$ and $HTaWO_6 \cdot 1/2H_2O$, as in Fig. 4a; and (c) sample heated 20 hr at 220°C, phase $HTaWO_6$.

(vi) Slight changes in the position of maxima occur for the two high energy bands. One of them shifts from 915 to 925 cm^{-1}, while the other one changes in the opposite way (from about 996 to 990 cm^{-1}). In addition a shoulder at about 1005 cm^{-1} appears. However, the most remarkable effect of moderate heating on the Raman spectrum seems to be the increase of relative intensity of the 990-cm^{-1} band.

(vii) The very broad band peaked in the hydrated form at about 2800 cm^{-1} disappears, as can be seen in Fig. 5b. A feature of compatible energy with an O–H stretching vibration survives at about 3300 cm^{-1} in a

sample treated at 300°C for 20 hr, which presents the same low-frequency Raman spectrum as Fig. 4b. These results should support an assignment of the former band to the stretching mode of H_2O molecules, while the latter could be associated to the O–H vibration of acidic protons.

Because of the relatively slight changes of the Raman spectrum, and taking into account the thermal study on phase relations, the phase obtained can be identified as dehydrated trirutile $HTaWO_6$

2.5.3. Unstable disordered phase. The spectrum of the disordered phase β, obtained from moderate heating of trirutile HTaWO6, has been already reported (*9*) for pellet samples, which underwent previously thermal treatments at 150°C to evaporate the organic solvent used for pelletizing process (Fig. 7a). In the present measurements on powders in glass capillary, a mixture of dehydrated $HTaWO_6$ and β phase is often shown by Raman spectra after treatments below 300°C (Fig. 7b).

The β-phase spectrum was also obtained by heating powders at about 400°C (Fig. 7c) and always appears in samples strongly irradiated by laser light (typical laser powers 300 mW or more), independently of the starting phase. Indeed, spectra of this kind were obtained by irradiating freshly exchanged powders, samples already in the stable dehydrated $TaWO_{5.5}$ phase (see next section), and even pyrochlore samples (*9*). In such cases the relative intensity of the highest frequency peak (about 1000 cm^{-1}) and the broad band centered at 720 cm^{-1} may show differences, probably related to the kinetics of evolution toward this phase. The transformation is completed when the sharp highest frequency peak is quenched. As already pointed out in the previous paper (*9*), the formation of this β phase is probably connected to surface effects, since it is revealed by Raman spectroscopy but not by bulk probes such as X-ray diffraction.

2.5.4. High-temperature evolution and Raman spectrum of $TaWO_{5.5}$. A clear, drastic and well reproducible modification of the

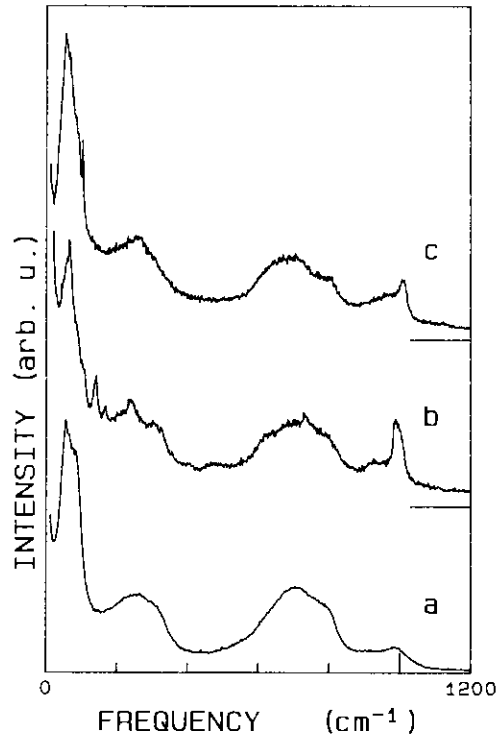

FIG. 7. Raman spectra of the disordered phase β, obtained under different conditions: (a) trirutile pellet samples, after thermal treatment at about 150°C; (b) trirutile powders, heated 67 hr at 150°C, (mixed with the ordered phase $HTaWO_6$); and (c) same trirutile powders, after heating 20 hr at 430°C.

Raman spectrum occurs when the samples are annealed in air for about 20 hr at temperatures between 400 and 600°C. A typical spectrum is shown in Fig. 4c and can be ascribed to the $TaWO_{5.5}$ phase on the basis of the thermal study reported in Section 2.1. All attempts to rehydrate the powder samples after the above thermal treatments failed, so that the water loss seems to be irreversible.

A few broad bands are observed, whose maxima occur at the same energy of sharp peaks of the hydrate ordered compound; this suggests a disorder-activated vibrational density of states. However, the characteristic highest frequency peak at 1000 cm^{-1} survives to this strong modification,

and seems to be less coupled to the lattice; i.e., it exhibits a narrower shape and a slightly increased frequency. The assignment of the spectrum to a fully dehydrated phase is confirmed by the absence of any O–H stretching vibration in the high frequency range.

A strong similarity of its overall shape to that of β-phase spectra is evident, but some minor differences should be considered (compare Figs. 4c and 7c). To complete the spectroscopic study of rutile-related $HTaWO_6$ phases successive annealings have been performed at 700 (see Fig. 4d), 800 (spectrum not shown), and 900°C (see Fig. 4e) on a powder sample. The annealings at 700°C seem to induce a transformation into a phase even more similar to β (see Fig. 4d, compared to spectra of Fig. 7), with a variance in the relative intensity for the highest frequency peak depending on the previous thermal history.

After the heating at 800 and 900°C (Fig. 4e), a new transformation takes place. According to the X-ray diffraction study, the structure of the new phase belongs to the tetragonal tungsten bronze (TTB) class. In the low-frequency Raman spectrum a new sharp peak arises at about 90 cm^{-1} and some broader features appear at about 320 and 800 cm^{-1}.

3. Discussion and Conclusions

The results of electrical conductivity and Raman scattering measurements are consistent with the phase relations within the $HTaWO_6 \cdot xH_2O$ trirutile-like system, as derived by thermal and crystallographic characterizations. The only unresolved point concerns the identification of β phase, detected by Raman spectroscopy during some thermal treatments. By considering the similarity of its spectrum to that of $TaWO_{5.5}$ (Fig. 4c), it would be natural to ascribe it to some disordered or amorphous modifications of such compound. Furthermore, the formation of this phase is probably just a surface process, and may occur apparently at temperatures somewhat lower than the stability range of bulky $TaWO_{5.5}$.

By comparison with the behaviour of the corresponding pyrochlore system, some relevant differences are observed.

First, the hydrated pyrochlore transforms into the anhydrous term $HTaWO_6$(p) in a single step, over a wide temperature range (25–230°C); $HTaWO_6$(p) remains stable up to 370°C, and then changes into $TaWO_{5.5}$(p) fairly quickly (370–450°C) (*1*). On the other hand, the hydrated trirutile dehydrates in two steps, and a true stability range for the $HTaWO_6$(t) phase can be hardly defined, since it promptly transforms into $TaWO_{5.5}$(t). Both polymorphs of $TaWO_{5.5}$ show with the X-ray diffraction a transition into a TTB-type phase above 800°C.

Second, the Raman measurements (see Fig. 5 of Ref. (*10*)) suggest that the $TaWO_{5.5}$(p) structure resembles that of the form $HTaWO_6 \cdot xH_2O$(p), with respect to the degree of order affecting the selection rules for the Raman scattering. On the contrary, the transition from the anhydrous form $HTaWO_6$(t) to the totally dehydrogenated $TaWO_{5.5}$(t) compound, observed reproducibly by Raman spectroscopy after treatments above 400°C, strongly changes the spectral shape (see for comparison Figs. 4b and 4c). However, the same spectrum appears for both forms, trirutile and pyrochlore, after heatings at 700°C, and can be related to the transition toward TTB structures. The spectral features appearing after the highest temperature annealings are very similar to the bands observed in strongly irradiated trirutile and pyrochlore samples (*10*). It cannot be excluded that such a phenomenon indicates at least at the sample surface, the transformation into a TTB structure.

The electrical conductivity of the hydrogenated trirutile phase is smaller by an order of magnitude than that of the corresponding pyrochlore compound. This is an important result, because it correlates well with the different structure type and the different stability of the two $HTaWO_6 \cdot xH_2O$ polymorphs. Unlike the case of the pyrochlore

compounds (*2, 3*), no neutron diffraction study has been performed on the trirutile phases, so that the details of their structures (including the H-atom positions) are not known. However, a consideration of the main topological features of both forms suggests that the layered configuration of trirutile should be less favourable for proton transport via a hopping mechanism than that of pyrochlore (based on tridimensional channels). Further experimental (neutron diffraction) and theoretical (H^+ potential energy maps) work is planned to clarify this point.

Acknowledgments

The authors thank Dr. E. Zanghellini for his skillful help in Raman measurements. Financial support from the Consiglio Nazionale delle Richerche (Rome) is also gratefully acknowledged.

References

1. C. M. Mari, F. Bonino, M. Catti, R. Pasinetti, and S. Pizzini, *Solid State Ionics* **18 & 19,** 1013 (1986).
2. D. Groult, J. Pannettier, and B. Raveau, *J. Solid State Chem.* **41,** 277 (1982).
3. F. J. Rotella, J. D. Jorgensen, B. Morosin, and R. M. Biefeld, *Solid State Ionics* **5,** 455 (1981).
4. M. Durand LeFloch, J. Pannetier, C. Doremieux-Morin, and H. Harribart, *J. Chem. Phys.* ***84,*** 4760 (1986).
5. E. Cazzanelli, G. Mariotto, M. Catti, and C. M. Mari, *Solid State Ionics* **46,** 135 (1991).
6. V. Bhat and J. Gopalakrishnan, *Solid State Ionics* **26,** 25 (1988).
7. V. Bhat and J. Gopalakrishnan, *J. Solid State Chem.* **63,** 278 (1986).
8. W. Viebahn, W. Rudorff, and H. Kornelson, *Z. Naturforsch. B* **22,** 1228 (1967).
9. E. Cazzanelli, G. Mariotto, M. Catti, and C. M. Mari, *Solid State Ionics* **53–56,** 383 (1992).
10. M. Catti, C. M. Mari, and G. Valerio, *J. Solid State Chem.* **98,** 269 (1992).
11. H. Ohtsuka, A. Yamaji, and T. Okada, *Solid State Ionics* **14,** 283 (1984).
12. N. Kumada, M. Takeshita, F. Muto, and N. Kinomura, *Mater. Res. Bull.* **23,** 1053 (1988).
13. C. M. Mari, A. Anghileri, M. Catti, ano G. Chiodelli, *Solid State Ionics* **28–30,** 642 (1988).
14. Most of the books on basic Raman theory. See, for example, H. Poulet and J. P. Mathieu, "Spectres de Vibration et Symmetrides Cristaux," Chap. VIII, Gordon & Breach, Paris, 1970.
15. E. Husson, Y. Repelin, H. Brusset, and A. Cerez, *Spectrochim. Acta Part A* **35,** 1177 (1979).
16. H. Haeuseler, *Spectrochim. Acta Part A* **37,** 487 (1981).
17. N. G. Eror and U. Balachandran, *Spectrochim. Acta Part A* **39,** 261 (1983).